

Dirac Cone Control in Two Dimensional Bilayer Graphene by Intercalation with Transition Metals

Srimanta Pakhira,^{†,‡} Kevin P. Lucht,^{†,‡} and Jose L. Mendoza-Cortes^{*,†,‡}

*Condensed Matter Theory, National High Magnetic Field Laboratory (NHMFL), Scientific
Computing Department, Materials Science and Engineering, Florida State University,
Tallahassee, Florida, 32310, USA.*

E-mail: mendoza@eng.famu.fsu.edu

Phone: +1-850-410-6298. Fax: +1-850-410-6150

Abstract

Bilayer graphene (BLG) is a pure semiconductor whose band gap and properties can be tuned by various methods such as doping or applying gate voltage. Here we show how the electronic properties of BLG can be tuned by intercalation of transition metal (TM) atoms between two monolayers graphene (MLG). We found that the symmetry, the spin and the concentration of TM atoms in BLG-intercalated materials are the important parameters to control and design a Dirac Cone in their band structures. Our study reveals that the BLG intercalated with one Vanadium (V) atom (BLG-1V) has a Dirac Cone at the K-point. We further examine this strategy for control in BLG

*To whom correspondence should be addressed

[†]Condensed Matter Theory, National High Magnetic Field Laboratory (NHMFL), Scientific Computing Department, Materials Science and Engineering, Florida State University, Tallahassee, Florida, 32310, USA.

[‡]Department of Chemical & Biomedical Engineering, FAMU-FSU Joint College of Engineering, and High Performance Materials Institute (HPMI), Florida State University, Tallahassee, Florida, 32310, USA.

intercalated with Nb and Ta. In all the cases, the present DFT calculations show that the $2p_z$ sub-shells of C atoms in graphene and the $3d_{yz}$ sub-shells of the V atoms provide the electron density near the Fermi level controlling the material properties of the BLG-intercalated materials. Thus we prove that out-of-plane atoms can influence in plane electronic densities in BLG, and enumerate what are the conditions to control the Dirac point. Thus, this study reveals a new strategy to control the material properties of BLG to exhibit various behaviors, including: metal, semi-metal, and semiconductor by varying the concentration and spin arrangement of the TM atoms in BLG.

In modern science and technology, there has been a tremendous amount of theoretical and experimental interest in the low energy electronic properties of ultrathin graphite films including graphene monolayer and graphene bilayer materials.¹⁻⁵ Graphene⁶, a 2D honeycomb sheet of carbon just one atom thick with hybridized sp^2 bonded orbitals between carbon atoms⁷, is an ideal and novel material for making nanoelectronic and photonic devices because it is a very good electrical conductor as well as being the thinnest 2D material known. Graphene has a unique linear band structure around the Fermi level (E_F) forming a Dirac Cone at the K-points of its Brillouin zone, and has led to fascinating phenomena, exemplified by massless Dirac fermion physics⁸⁻¹¹. This emergent behavior of Dirac fermions in condensed matter systems defines the unifying framework for a class of materials called Dirac materials.

Monolayer graphene (MLG) or graphene has an electronic structure that can be controlled by an electrical field¹². To be used in digital electronics, however, MLG has the well known zero-gap issue¹³ which makes a high on-off ratio difficult; deeming it unsuitable for transistors, which are the foundation of all modern electronic devices. Bilayer graphene (BLG) can be used instead of MLG to overcome the zero-gap problem, with a gap opening simply by applying an electric field^{14,15}. BLG has an entirely different band structure, and equally interesting^{16,17}, since the band gap of the BLG can be modulated from zero to a few eV by using different methods such as doping and applying an external electric field. In addition,

BLG holds the potential for electronics and nano-technological applications, particularly because of the possibility to control both carrier density and energy band gap through doping or gating^{8,9,17-19}. The most remarkable property of BLG is that the inversion symmetric AB-stacked BLG is a zero-band gap semiconductor in its pristine form, but a non-zero band gap can be induced by breaking the inversion symmetry of the two graphene monolayers to form AA-stacked BLG. When two graphene monolayers are stacked (in both the cases AA- and AB-stacked), the monolayer features are lost and dispersion effects become quadratic and more effective¹⁸. Thus, BLG acts as a semiconductor and exhibits an induced electric field and broadly tunable band gap^{9,20}. Because tuning the band gap of BLG can turn it from a semiconductor into a metal or semi-metal, a single millimeter-square sheet of BLG could potentially hold millions of differently tuned electronic devices that can be reconfigured. Recently, lasers have been used to get BLG to act as: a conductor, a Dirac material or a semiconductor; an important step towards computer chips made of a 2D material²¹.

In this article, we show that the Dirac Cone in the band structure of BLG can be controlled by adding transition metal (TM) atoms between two graphene layers (here we used Vanadium (V), Tantalum (Ta) and Niobium (Nb) metal atoms) so that the electronic band gap between the valence and conduction bands can be tuned; thus resulting in the appearance of a Dirac Cone only in BLG-1V. By definition; intercalation occurs when metal atoms are inserted between two graphene monolayers. Intercalation of the TM atoms and their spins causes a surprisingly diverse array of electronic properties. Additionally, the band gap depends on the coupling between the two graphene layers and symmetry of the BLG system i.e. AB stacking vs AA stacking. We have performed a theoretical investigation of the electronic properties such as band structure, projected density of states (DOSs), spin arrangements, and structural stability of MLG, BLG, BLG intercalated with one Vanadium atom (BLG-1V), BLG intercalated with two Vanadium atoms (BLG-2V), and BLG intercalated with three Vanadium atoms (BLG-3V) per unit cell as shown in Figure 1. Their structural stabilities are also reported as Gibbs free energies (ΔG_f).

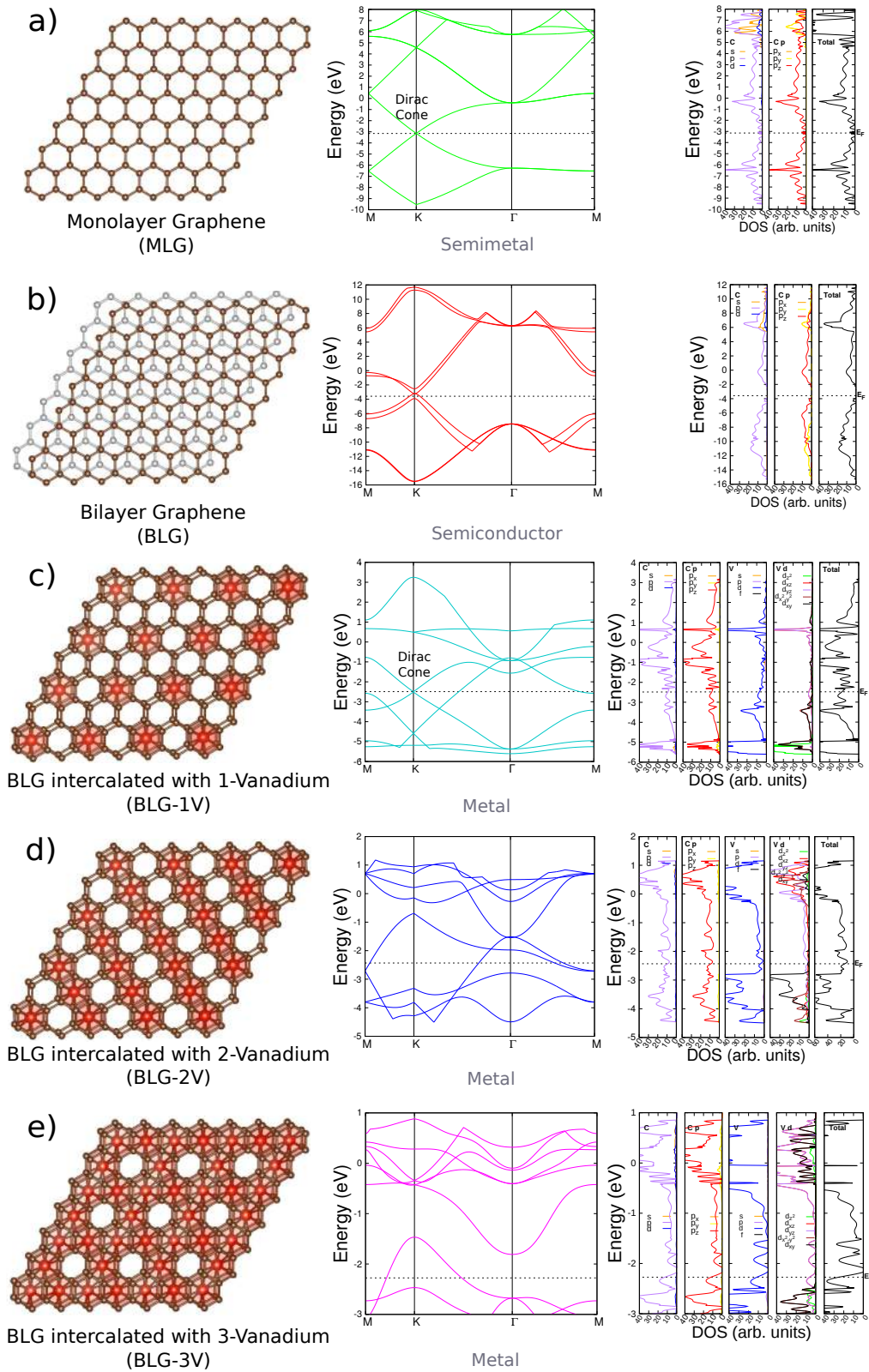


Figure 1: The optimized structures, band structures and density of states (DOSs) are shown a) MLG, b) BLG, c) BLG-1V, d) BLG-2V, and e) BLG-3V. The individual components of the DOSs of the C and V atoms and total DOSs (depicted by "Total") are also presented in here. The energy for the band structures and DOSs is reported with respect to vacuum

The geometry of the 2D layer structures MLG, BLG and BLG-intercalated materials (BLG-1V, BLG-2V, BLG-3V and BLG-1Nb and BLG-1Ta) were optimized by dispersion-corrected unrestricted hybrid density functional theory²²⁻²⁷, i.e. UB3LYP-D2, which has been shown to give correct electronic properties for 2D materials^{25,28}. During the optimization and single point energy calculations, ‘SPIN’ and ‘SPINLOCK’ keywords were used to specify the unrestricted wave functions and the total spin of the BLG-intercalated materials, respectively. The ‘ATOMSPIN’ keyword was also used to specify the individual spins of the TM atoms in the BLG-intercalated materials. The semi-empirical Grimme-D2 dispersion corrections were added in the present calculations in order to incorporate van der Waals dispersion effects on the system.²⁵⁻²⁷ The CRYSTAL14²⁹ suite code was used to perform all the computations. The bilayer graphene intercalated 2D materials (BLG-1V, BLG-2V, BLG-3V and BLG-1Nb and BLG-1Ta) have been prepared by adding the V, Nb and Ta atoms in one unit cell of the crystal structures. In the present computation, triple-zeta valence with polarization quality (TZVP) Gaussian basis sets were used for both C and V³⁰, and HAYWSC effective core potentials (ECP) were used for both Nb and Ta³¹.

Integration inside of the first Brillouin zone were sampled on 15 x 15 x 1 k-mesh grids for all the materials for both the optimization and material properties (band structures and density of states) calculations with a resolution of around $2\pi \times (1/60) \text{ \AA}^{-1}$ for all bilayer graphene intercalated materials, and $2\pi \times (1/40) \text{ \AA}^{-1}$ for MLG. We have plotted the bands along a high symmetric k-direction, M – K – Γ – M, in the first Brillouin zone. Electrostatic potential calculations have been included in the present computation i.e. the energy for the band structures and DOSs is reported with respect to vacuum. The BLG unit cell constructed this way contains one configuration, known as AA, where one atom is exactly above another atom of the other layer of graphene (see Figure S1). There is another BLG configuration, AB, where an atom of the top of graphene layer is exactly in the center of a lower layer hexagon as shown in Figure 1b. To reproduce previous experimental and theoretical results, we have considered both AA and AB-stacking BLG. The optimized geometries of MLG, AB-

stacked BLG, BLG-1V, BLG-2V and BLG-3V materials along with their band structures and projected density of states (DOSs) are shown in Figure 1a-e. The optimized geometry, band structures and DOSs of pristine AA-stacked BLG are reported in the Supporting Information (see Figure S1). The contribution of the sub-shells (such as p_x , p_y , p_z , d_{yz} etc.) in the total DOSs has been also computed for all the cases as shown in the right side of Figure 1.

The present DFT calculation shows that the Dirac Cone exists at the K-point in the band structure of MLG which is consistent with previous results⁸⁻¹¹. For this case, the valence bands of MLG arise from the $2p_z$ sub-shells of C atoms, which make the Dirac Cone (see Figure 1a). The total DOSs calculations show a small electron density around the Fermi energy level (E_F), confirming MLG as a semimetal.

For the pristine AB-stacked BLG, the Fermi level lies below the point where the valence and conduction bands touch each other as shown in Figure 1b. Our present computation shows that AB-stacked BLG is thermodynamically more stable than the AA-stacked BLG. The valence and conduction bands are crossing the E_F at the K-points for both the AA- and AB-stacked BLG. Thus, both the AA- and AB-stacked BLG have no Dirac Cone, which agree well with the previous experimental results^{32,33}, i.e. the AA-/AB-stacked BLG materials are ordinary non-zero/zero band gap semiconductors; see Figure S1 and Figure 1b, respectively. The bond distances, lattice constants (a and b), and intercalation distance (d) are reported in Table 1. The distance between the two monolayers in the pristine AB-stacked BLG material is about 3.390 Å which agrees with the previous experimental and theoretical results³². We have also calculated the binding energy (ΔG_f) of all the system studied here as shown in Table 2. The binding energy, ΔG_f , to form the AB-stacked BLG from two MLG, is about -0.86 eV.

The optimized structure between Vanadium and graphene follows an AA-stacking arrangement with the Vanadium placed at the center of the honeycomb, which forms BLG-1V. On this conformation, the Vanadium d -orbitals will be situated to favorably interact with

Table 1: Bond distances and lattice constants for MLG, BLG, BLG-1V, BLG-2V, and BLG-3V materials. The d is defined as the interlayer distance between the monolayers.

Component	C-C (\AA)	C-V (\AA)	a (\AA)	b (\AA)	d (\AA)
MLG	1.416	N/A	2.451	2.451	N/A
AA-stacked BLG	1.414	N/A	2.449	2.449	3.201
AB-stacked BLG	1.421	N/A	2.449	2.449	3.390
BLG-1V	1.439	2.243	4.942	4.942	3.441
BLG-2V	1.442	2.335	8.575	5.022	3.645
BLG-3V	1.464	2.413	5.032	5.032	3.658

Table 2: Relevant properties of the MLG, BLG, BLG-1V, BLG-2V, and BLG-3V; the binding energy, ΔG_f , is with respect to their individual components: MLG and V atoms.

Component	State	ΔG_f (eV)	Dirac Cone
MLG	Semimetal	N/A	Yes
AA-stacked BLG	Semiconductor	-0.78	No
AB-stacked BLG	Semiconductor	-0.86	No
BLG-1V	Metal	-5.97	Yes
BLG-2V	Metal	-5.67	No
BLG-3V	Metal	-5.36	No

the p_z orbital orthogonal of the graphene layer. The BLG-1V structure is highly favorable by -5.97 eV relative to BLG and one free V atom. Additional Vanadium atoms are also favorable to further intercalation by -5.67 eV between single and double metal addition to form BLG-2V, and by -5.36 eV between the double and triple metal addition to form BLG-3V as shown in Table 2. The present DFT calculations show that the intercalation distances have been gradually increased when more V atoms are added from BLG-1V to BLG-3V, but not equally as shown in Table 1. Our computation also shows the C-C bond distance has been increased by an average of 0.014 \AA in BLG-1V, BLG-2V and BLG-3V due to the presence of V atoms between the graphene layers compared to BLG. We have calculated the stability of BLG intercalated with four V atoms (BLG-4V), but the frequency calculations show that the structure is unstable thermodynamically as it has many imaginary frequencies, and hence this result is excluded from this article.

The addition of Vanadium atoms was found to substantially alter the electronic properties of graphene bilayer. The addition of a single Vanadium atom intercalated in AA-stacked BLG

(i.e. BLG-1V) yields a Dirac Cone along the K-direction as shown in Figure 1c. The DOSs around the Fermi energy level indicates metallic behavior. The individual components of the p -orbitals electron density for C atoms and the d -orbitals electron density for V atoms have been explicitly shown along with the total DOSs in Figure 1c. The density projections show the electrons can freely move from the valence band to the conduction band, and it reveals the intrinsic electron mobility for BLG-1V. The DOSs calculations for BLG-1V show the electron density around the E_F is coming from the p_z sub-shells of C atoms in graphene (highlighted by red color) and the d_{yz} sub-shell of V atom (highlighted by violet color). In other words, the p_z sub-shell of carbon, and d_{yz} sub-shells of vanadium is mostly responsible for the emergence of the Dirac Cone in BLG-1V. In MLG, the Dirac cone comes from p -orbitals of C atoms alone, but for BLG-1V, the nature of the Dirac cone might be different because it might come from the p -orbitals alone of BLG, or d -orbitals alone of the V atom or $p - d$ hybridized orbitals of C and V atoms. To resolve this, we use the coordinates of the optimized geometry of BLG-1V, and then (i)- removed the BLG layer, and in another calculations (ii)- remove the V atoms. We then calculate the electronic properties of these structures (Figure S2). The band structure shows that the Dirac cone disappears when only the V atoms are used and also when only BLG is used. In the BLG case the Dirac point still exist but it has shifted above E_F , just like in the ideal AA-stacked BLG. This suggest that $p - d$ hybridized orbitals are the source for the Dirac cone in BLG-1V. As an excellent conductor and Dirac material, BLG-1V can be used in various modern electronic devices.

BLG-2V and BLG-3V can be formed with the addition of one V and two V atoms to the BLG-1V material, respectively. Different spin states of BLG-2V and BLG-3V have been considered but only the most stable configurations are discussed here, while the other less stable spin states are discussed in the SI. First, we discussed the Ferromagnetic (FM) state for both materials, which results in the Dirac Cone disappearing, and the bands to shift, showing a metallic behavior when the spins of Vanadium atoms align. Interestingly, in general for all these materials in the FM state, the $3d$ orbitals of V receive more electron donation from the

graphene $2p_z$ sub-shells when the total spin is increased. The band structure reveals that along the M to K directions, the valence band crosses the Fermi level in both BLG-2V and BLG-3V resulting in large electron distribution around the Fermi level as shown in Figure 1d and Figure 1e, respectively. Thus, both BLG-2V and BLG-3V show metallic behavior as depicted in their total DOSs. In both materials, the total DOSs show that electron density around the Fermi level is due to the p_z sub-shell electrons from C atoms in graphene and the d_{yz} sub-shell electrons from V atoms as depicted in the sub-shells DOSs calculations (see Figure 1d - 1e).

The other relevant arrangement for both BLG-2V and BLG-3V is anti-ferromagnetic (AFM) state, which is now briefly discussed. By considering an AFM arrangement of spins, we can drastically modify the properties of BLG-2V. The spin conformations of all the BLG-intercalated materials are reported in Table S1. Figure 2 shows the band structure and DOSs of the AFM state for BLG-2V. To further analyze the wave function, we calculate the Mulliken spin population analysis. In the case of BLG-2V, the AFM conformation yielded higher spin of individual V atoms, 2.22 and -2.22 compared to the FM conformation with 1.86 for each Vanadium. Thus the average total spin of AFM BLG-2V material is 0.0. Relative to its FM counterpart, the AFM BLG-2V structure is more stable by $\Delta G_f = 0.410$ eV. Examining the electronic properties, we noticed considerable differences between the AFM and FM BLG-2V material properties and their structures. Once in the AFM state, BLG-2V have a degenerate pair of band structures (for alpha and beta electrons) with a band opening between the valence and conduction bands. The band gaps are 0.101 eV for the indirect transition and 0.681 eV for the direct transition. The most important finding is that by altering the spin, the AFM BLG-2V material becomes a semiconductor which may be useful for modern electronic devices. Thus this calculation reveals that a band gap can be introduced in BLG-2V by altering the spin alignment of the intercalated V atoms. The AFM conformation for BLG-3V was also found, but it is not as interesting as AFM BLG-2V (Figure S3 and SI).

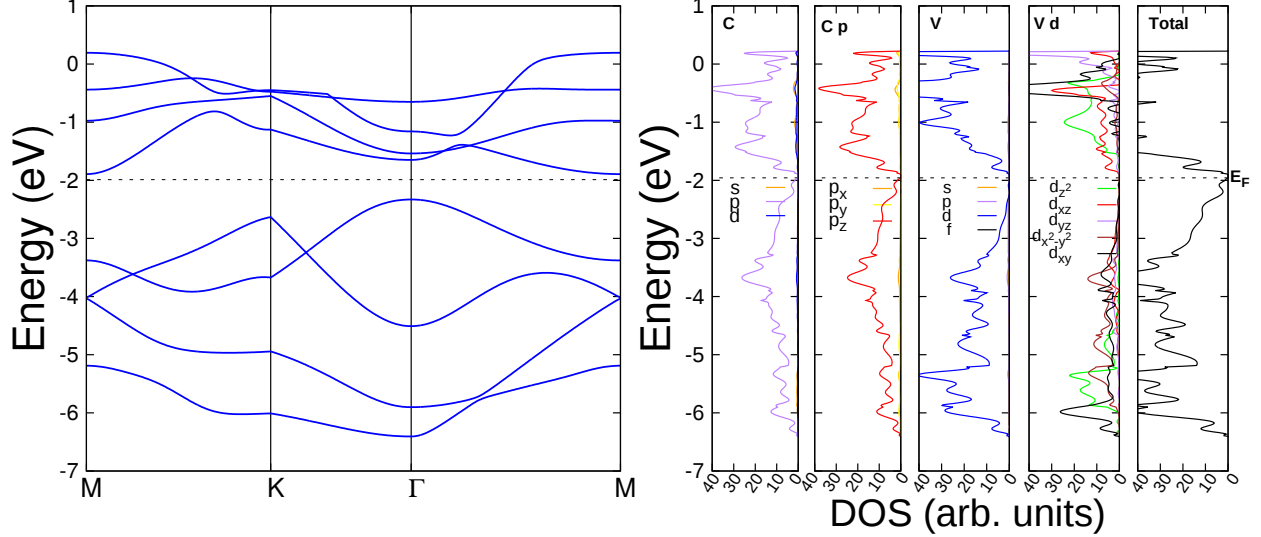


Figure 2: Band structure and DOSs of the alpha electron in AFM state for BLG-2V are presented. The beta electrons exhibit identical information. The individual and total components of DOSs of the C and V atoms are also shown. Compared to the FM state, in the AFM state a band gap appears.

We further extended our studies on the equilibrium structures and electronic properties of Niobium (Nb) and Tantalum (Ta) intercalated BLG materials: BLG-1Nb and BLG-1Ta to investigate if the Dirac Cone exists or not in these materials; see Figure 3. The structural parameters of both materials are reported in Table S2. The DFT calculations found that the intercalation distance d was increased in both materials compared to BLG-1V by at least 0.1 \AA , which is consistent with Nb and Ta being larger than V. It also indicates that the interaction between the Nb or Ta and graphene layers in both BLG-1Nb and BLG-1Ta is weaker than in BLG-1V, which can be further corroborated by the ΔG_f . The electronic properties of both materials are shown in Figure 3. The band structure calculations showed that they have no Dirac Cone but instead the Dirac point moved above the E_F . The total DOSs calculation found that the electron densities are large around the E_F , which are coming from the p -subshells of C atoms and d -subshell of Nb and Ta atoms as depicted in Figure 3. These calculations also showed that they have metallic behavior and thus they are conductors.

We have investigated why the Dirac Cone does not exist in BLG-1Nb and BLG-1Ta but

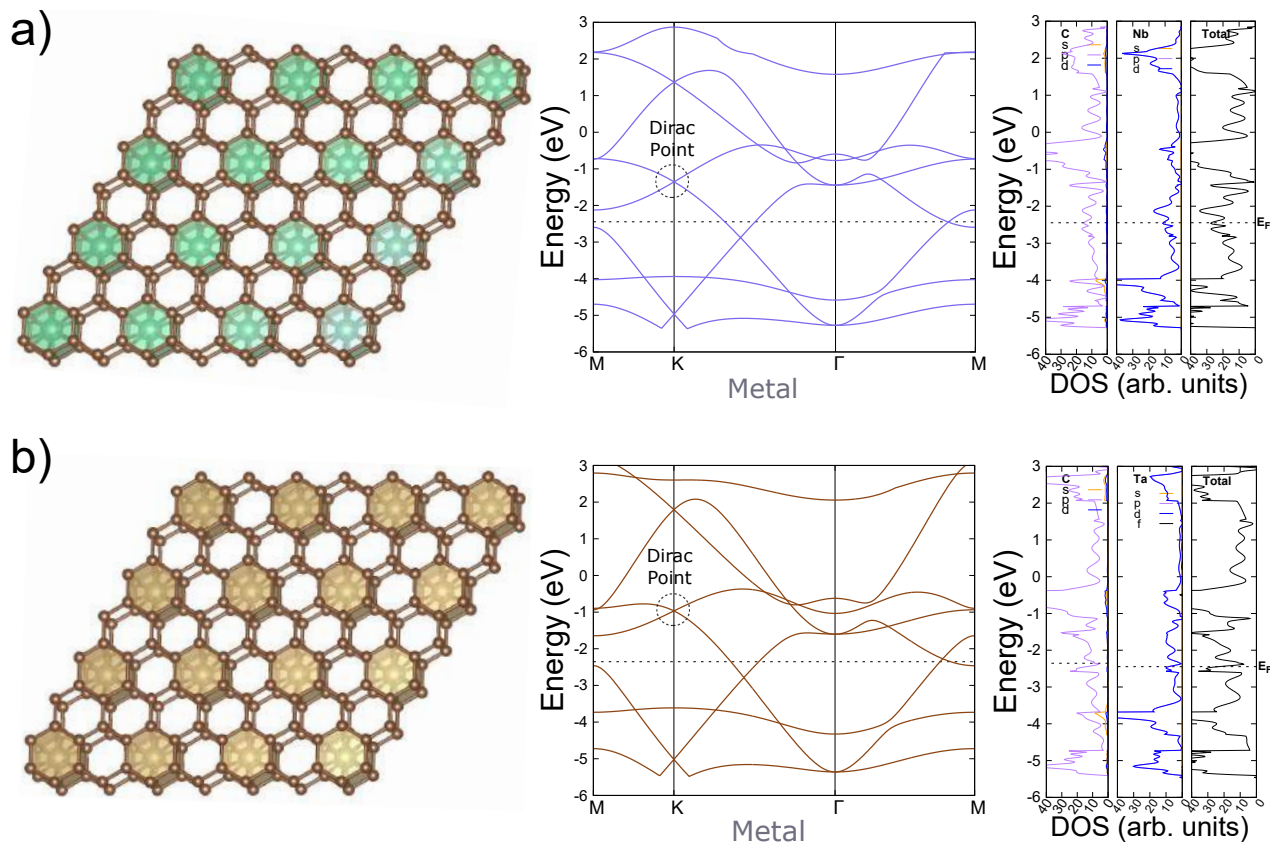


Figure 3: The optimized structures, band structures and density of states (DOSs) are shown for a) BLG-1Nb, and b) BLG-1Ta. The individual components of the DOSs of the C, Nb and Ta atoms and total DOSs (depicted by “Total”) are also presented in here.

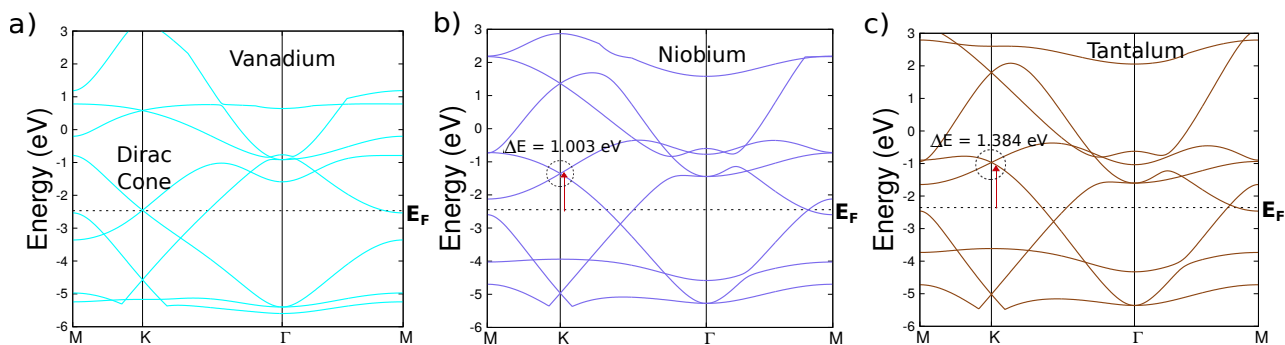


Figure 4: Comparison of band structures of a) BLG-1V, b) BLG-1Nb, and b) BLG-1Ta showing how the Dirac point remains but it is shifted up with respect to the E_F .

the Dirac point still does, by studying Mulliken population analysis and spin density analysis. The BLG-1V, BLG-1Nb and BLG-1Ta materials have the $p6/mmm$ layer symmetry which is the same to monolayer graphene. The Mulliken spin population analysis finds that the total spin of BLG-1V is 2.082 with vanadium having a spin of 2.245. Whereas the total spins of BLG-1Nb and BLG-1Ta are 1.399 and 1.294, with niobium and tantalum having spins of 1.245 and 1.068, respectively. These calculations show that the number of unpaired electrons are decreasing when we intercalated heavier atoms such as Nb and Ta in bilayer graphene. Thus we can say that the Dirac cone has moved away from the Fermi level as shown in Figure 4. The present DFT calculations found the band crossing points in the band structures of BLG-1Nb and BLG-1Ta are shifted by 1.003 eV and 1.384 eV, respectively as depicted in Figure 4. Thus the individual unpaired electrons of V, Nb and Ta play an important role in order to have a Dirac Cone in the band structures of the BLG intercalated materials. The BLG-2V material lost the $p6/mmm$ layer symmetry, thus the Dirac point can not be present and the concentration of V atoms increased, as a consequence the metal features dominate (Figure 1d). Apart from the spin, and symmetry, the concentration of the metal atoms in the BLG system is another important factor. BLG-3V has the same symmetry ($p6/mmm$) but the concentration of V atoms increased; thus the symmetry allows it to have graphene features which do not show around E_F , because around it, mostly features of the metal are present. In other words, it loses the Dirac Cone because of the dominance of the metal concentration as displayed in Figure 1e.

We have studied the structure and material properties of the MLG, BLG, BLG-intercalated nanostructured 2D materials. The individual components of the p -subshell of C atoms and the d -subshell of the V, Nb, Ta atoms are reported along with the total DOSs. Among all the systems, MLG and BLG-1V materials have a Dirac Cone at the K-point. Once the concentration of Vanadium is increased the Dirac Cone disappears. We have also found that the $2p_z$ sub-shell of C atoms and $3d_{yz}$ sub-shell of the V atoms in the BLG-1V, BLG-2V, and BLG-3V materials are the main components around E_F playing the main role to show the

Dirac Cone and the conducting properties. Thus we have shown that the control of the Dirac Cone on the intercalated BLG is a delicate balance between the amount of unpaired electrons concentration of the TMs and symmetry. This means that the layer symmetry ($p6/mmm$) is necessary for the Dirac point to appear in graphene-like materials (BLG-1V, BLG-1Nb and BLG-1Ta), however E_F is controlled by the number of unpaired electrons. In other words, if the concentration of TMs is too high, even having the same symmetry ($p6/mmm$) will not be sufficient to keep the Dirac point at the E_F , because the band features will be dominated by the metal. This is clearly shown on how the material properties have been changed in BLG-1V, and BLG-3V due to the presence of Vanadium atoms using the same symmetry. The nature of the Dirac cone in MLG and BLG-1V is different, materials massless fermions leading to ultrahigh carrier mobility, with the former having p -orbitals character while the second involves p - and d - orbitals. In conclusion, the Dirac point can be present in BLG intercalated with TM by controlling symmetry and concentration of electrons, with this guidelines succeeding at controlling a Dirac point in the BLG-1V material.

Acknowledgement

S.P. and J.L.M-C. were supported by Florida State University (FSU). S.P. and J.L.M-C. gratefully acknowledges the support from the Energy and Materials Initiative at FSU. S.P. is grateful to Dr. Yohanes Pramudya and Mr. Oluwagbenga Iyiola from FSU for helpful discussions and guidance with computational resources. The authors thank the High Performance Computer cluster at the Research Computing Center in FSU, for providing computational resources and support.

Supporting Information Available

The supporting Information is available free of charge on the ACS Publications website.
Section 1: Optimized geometry, band structure and density of states of AA-stacked bilayer

graphene. Section 2: Nature of the Dirac Cone in BLG-1V. Section 3: Effect of spin alignment on BLG-3V material. Section 4: Optimized Structures (.cif format). This material is available free of charge via the Internet at <http://pubs.acs.org/>.

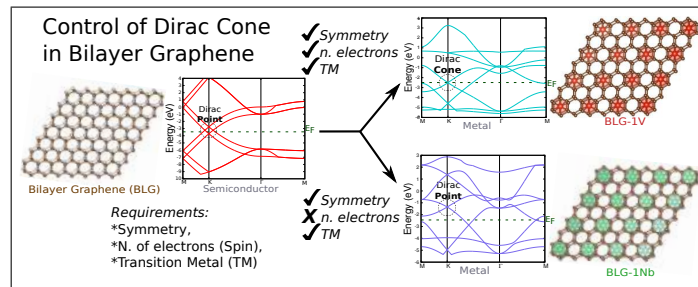
References

- (1) Novoselov, K. S.; Geim, A. K.; Morozov, S. V.; Jiang, D.; Katsnelson, M. I.; Grigorieva, I. V.; Dubonos, S. V.; Firsov, A. A. *Nature* **2005**, *438*, 197–200.
- (2) Kim, N.; Kim, K. S.; Jung, N.; Brus, L.; Kim, P. *Nano Letters* **2011**, *11*, 860–865.
- (3) Tan, L. Z.; Park, C.-H.; Louie, S. G. *Nano Letters* **2011**, *11*, 2596–2600.
- (4) Szafranek, B. N.; Schall, D.; Otto, M.; Neumaier, D.; Kurz, H. *Nano Letters* **2011**, *11*, 2640–2643.
- (5) Yan, H.; Low, T.; Guinea, F.; Xia, F.; Avouris, P. *Nano Letters* **2014**, *14*, 4581–4586.
- (6) Novoselov, K. S. et al. *Science* **2004**, *306*, 666–669.
- (7) Castro Neto, A. H.; Guinea, F.; Peres, N. M. R.; Novoselov, K. S.; Geim, A. K. *Reviews of Modern Physics* **2009**, *81*, 109–162.
- (8) Ohta, T. *Science* **2006**, *313*, 951–954.
- (9) Castro, E. V.; Novoselov, K. S.; Morozov, S. V.; Peres, N. M. R.; Dos Santos, J. M. B. L.; Nilsson, J.; Guinea, F.; Geim, A. K.; Neto, A. H. C. *Physical Review Letters* **2007**, *99*, 8–11.
- (10) Zhou, S. Y.; Gweon, G.-H.; Fedorov, a. V.; First, P. N.; de Heer, W. a.; Lee, D.-H.; Guinea, F.; Castro Neto, a. H.; Lanzara, a. *Nature materials* **2007**, *6*, 770–775.
- (11) Mullen, K.; Uchoa, B.; Glatzhofer, D. T. *Physical Review Letters* **2015**, *115*, 1–5.

- (12) Novoselov, K. S.; Fal'ko, V. I.; Colombo, L.; Gellert, P. R.; Schwab, M. G.; Kim, K. *Nature* **2012**, *490*, 192–200.
- (13) Avouris, P. *Nano Letters* **2010**, *10*, 4285–4294.
- (14) Oostinga, J. B.; Heersche, H. B.; Liu, X.; Morpurgo, A. F.; Vandersypen, L. M. K. *Nature materials* **2008**, *7*, 151–157.
- (15) McCann, E. *Physica Status Solidi (B) Basic Research* **2007**, *244*, 4112–4117.
- (16) Ohta, T.; Bostwick, A.; McChesney, J. L.; Seyller, T.; Horn, K.; Rotenberg, E. *Physical Review Letters* **2007**, *98*, 16–19.
- (17) Nath, P.; Sanyal, D.; Jana, D. *Current Applied Physics* **2015**, *15*, 691–697.
- (18) McCann, E.; Fal'ko, V. I. *Physical Review Letters* **2006**, *96*, 1–4.
- (19) Novoselov, K. S.; McCann, E.; Morozov, S. V.; Falko, V. I.; Katsnelson, M. I.; Zeitler, U.; Jiang, D.; Schedin, F.; Geim, a. K. *Nat. Phys.* **2006**, *180*, 177–180.
- (20) Choi, S.-M.; Jhi, S.-H.; Son, Y.-W. *Nano Letters* **2010**, *10*, 3486–3489.
- (21) Lin, Z.; Ye, X.; Han, J.; Chen, Q.; Fan, P.; Zhang, H.; Xie, D.; Zhu, H.; Zhong, M. *Scientific reports* **2015**, *5*, 11662.
- (22) Becke, A. D. *The Journal of Chemical Physics* **1993**, *98*, 5648.
- (23) Becke, A. D. *Physical Review A* **1988**, *38*, 3098–3100.
- (24) Lee, C.; Yang, W.; Parr, R. G. *Physical Review B* **1988**, *37*, 785–789.
- (25) Grimme, S. *Journal of Computational Chemistry* **2006**, *27*, 1787–1799.
- (26) Pakhira, S.; Sahu, C.; Sen, K.; Das, A. K. *Chemical Physics Letters* **2012**, *549*, 6–11.
- (27) Pakhira, S.; Sen, K.; Sahu, C.; Das, A. K. *The Journal of Chemical Physics* **2013**, *138*, 164319.

- (28) Lucht, K. P.; Mendoza-Cortes, J. L. *Journal of Physical Chemistry C* **2015**, *119*, 22838–22846.
- (29) Dovesi, R.; Orlando, R.; Erba, A.; Zicovich-Wilson, C. M.; Civalleri, B.; Casassa, S.; Maschio, L.; Ferrabone, M.; De La Pierre, M.; D'Árco, P.; Noel, Y.; Causa, M.; Rerat, M.; Kirtman, B. *International Journal of Quantum Chemistry* **2014**, *114*, 1287–1317.
- (30) Peintinger, M. F.; Oliveira, D. V.; Bredow, T. *Journal of Computational Chemistry* **2013**, *34*, 451–459.
- (31) Dall'olio, S.; Dovesi, R.; Resta, R. *Physical Review B* **1997**, *56*, 10105–10114.
- (32) Min, H.; Sahu, B.; Banerjee, S. K.; MacDonald, A. H. *Physical Review B - Condensed Matter and Materials Physics* **2007**, *75*, 1–7.
- (33) Latil, S.; Henrard, L. *Physical Review Letters* **2006**, *97*, 1–4.

Graphical TOC Entry



Supplementary Information

Dirac Cone Control in Two Dimensional Bilayer Graphene by Intercalation with Transition Metals

Srimanta Pakhira^{1,2}, Kevin P. Lucht^{1,2}, Jose L. Mendoza-Cortes^{1,2}

¹ Condensed Matter Theory, National High Magnetic Field Laboratory, Scientific Computing Department, Materials Science and Engineering, Florida State University (FSU), Tallahassee, Florida, 32310, USA

² Department of Chemical & Biomedical Engineering, FAMU-FSU Joint College of Engineering, and High Performance Materials Institute (HPMI), Florida State University, Tallahassee, Florida, 32310, USA.

E-mail: mendoza@eng.famu.fsu.edu

Contents

	Page
Title	S1
List of Contents	S2
List of Figures	S3
1 Optimized geometry, band structure and density of states of AA-stacked bilayer graphene . .	S4
2 Nature of the Dirac Cone in BLG-1V	S5
3 Effect of spin alignment on BLG-3V material	S6
4 Optimized Structures (.cif format)	S7
4.1 MLG: Monolayer Graphene	S7
4.2 AA-BLG: AA-stacked Bilayer Graphene	S8
4.3 AB-BLG: AB-stacked Bilayer Graphene	S9
4.4 BLG-1V: BLG-intercalated with 1 V	S10
4.5 BLG-2V: BLG-intercalated with 2 V	S11
4.6 BLG-3V: BLG-intercalated with 3 V	S12
4.7 BLG-1Nb: BLG-intercalated with 1 Nb	S13
4.8 BLG-1Ta: BLG-intercalated with 1 Ta	S13

List of Figures

	Page
S1 The optimized structures of AA-stacked bilayer graphene (BLG).	S4
S2 Electronic properties and geometry for BLG-1V, BLG-1V with the BLG removed and BLG-1V with the V atom removed	S5
S3 Band structure and DOSs of the alpha electron of AFM BLG-3V	S6
S4 Band structure and DOSs of the beta electron of AFM BLG-3V	S7

1 Optimized geometry, band structure and density of states of AA-stacked bilayer graphene

The optimized structure, band structures and density of states (DOSs) of AA-stacked bilayer graphene (BLG) are shown in Figure S1. The band and DOSs calculations reveal that AA-stacked BLG is a non-zero band gap semiconductor, and it has an indirect band gap around 0.25 eV as depicted in the band structure. Notice that the band structure does not show the gap, but the band gap is reported based on the DOS calculations. The individual components of p-orbital (i.e. p_x , p_y and p_z sub-shells) are calculated along with total DOSs. We found the p_z sub-shell of p-orbital accounts for the largest electron contribution in the total DOSs.

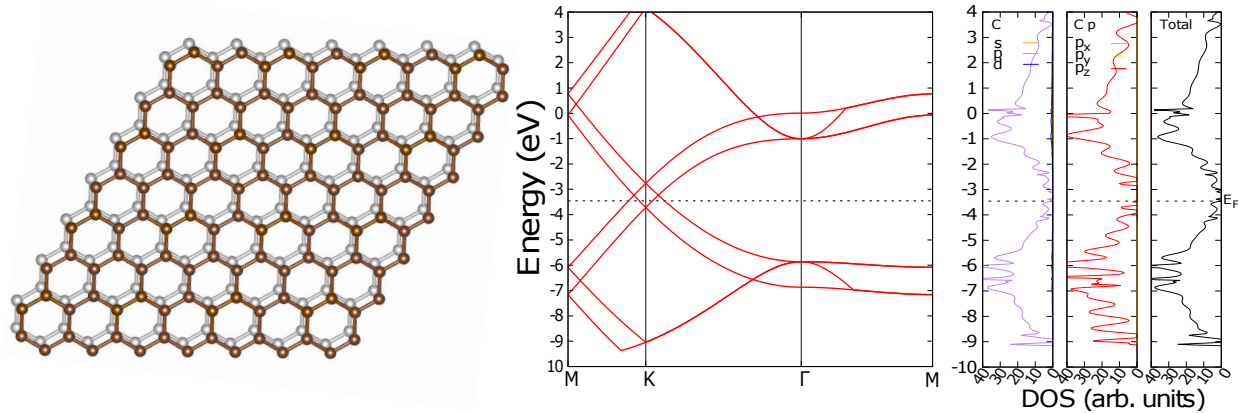


Figure S1: The optimized structure, band structure and density of states (DOSs) of AA-stacked BLG are shown. The individual components of DOSs of the C atom, and total DOSs (depicted by “Total” in the third column) are also presented.

2 Nature of the Dirac Cone in BLG-1V

In MLG, the Dirac Cone comes from p -orbitals of C atoms alone, but for BLG-1V, the nature of the Dirac Cone might be different because it might come from the p -orbitals alone, or d -orbitals alone or $p-d$ hybridized orbitals. To resolve this, we use the optimized geometry of BLG-1V, and then 1.- removed the BLG layer and 2.- remove the V atoms, and the results are shown in Figure S2. Notice how the Dirac Cone disappears when only the V atoms are used Figure S2b. The same occurs when only the BLG is used, Figure S2c, however in this case the Dirac Cone is still present but is has shifted above E_F . The results suggest that $p-d$ hybridized orbitals are the source for the Dirac cone in BLG-1V.

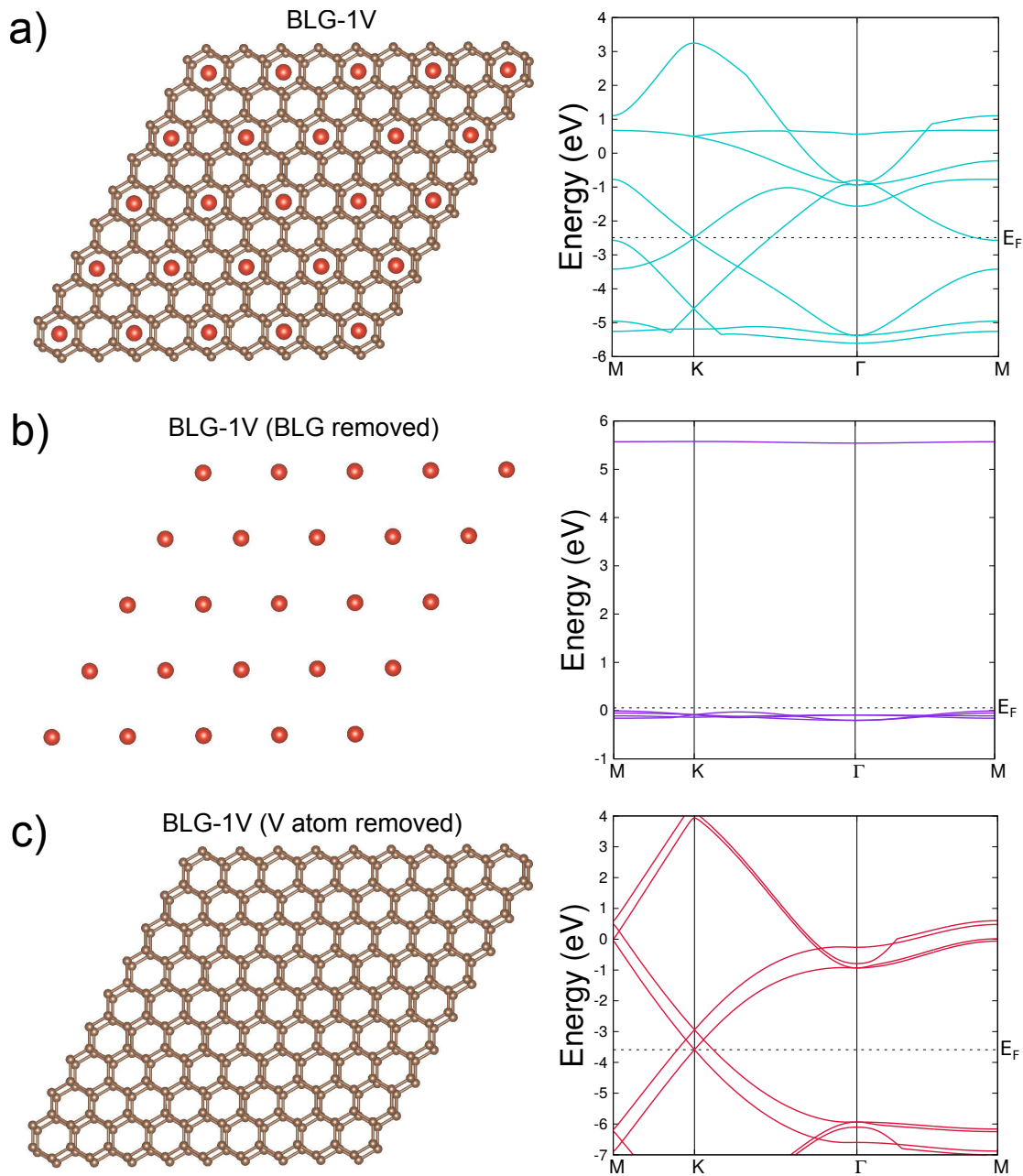


Figure S2: Electronic properties (left) and geometry (right) for a) BLG-1V, b) BLG-1V with the BLG removed and c) BLG-1V with the V atom removed

3 Effect of spin alignment on BLG-3V material

An alternative method of controlling the electronic properties of BLG-intercalated materials is by altering the spin configuration. We carried out Mulliken spin density analysis to study the spin configuration. The estimation of spin might vary using another method. All previous materials have referenced Vanadium in the high-spin state, and in the case of BLG-2V and BLG-3V in a ferromagnetic (FM) spin arrangement. Considering an anti-ferromagnetic (AFM) arrangement of spins, we can drastically modify the properties. The AFM arrangement of the BLG-2V was reported in the main manuscript. Here we showed the spin conformations of the BLG-2V and BLG-3V materials, and the Mulliken spin densities of the V atoms in the BLG-intercalated materials are reported in Table S1.

Table S1: Different Mulliken spin population of the BLG-intercalated materials.

Materials	Average Spin of V	Total Spin
BLG-1V	2.245	2.082
FM BLG-2V	1.856	3.740
FM BLG-3V	1.489	4.375
AFM BLG-2V	0.000 (2.215, -2.215)	0.000
AFM BLG-3V	0.157	0.405
BLG-1Nb	1.245	1.399
BLG-1Ta	1.068	1.294

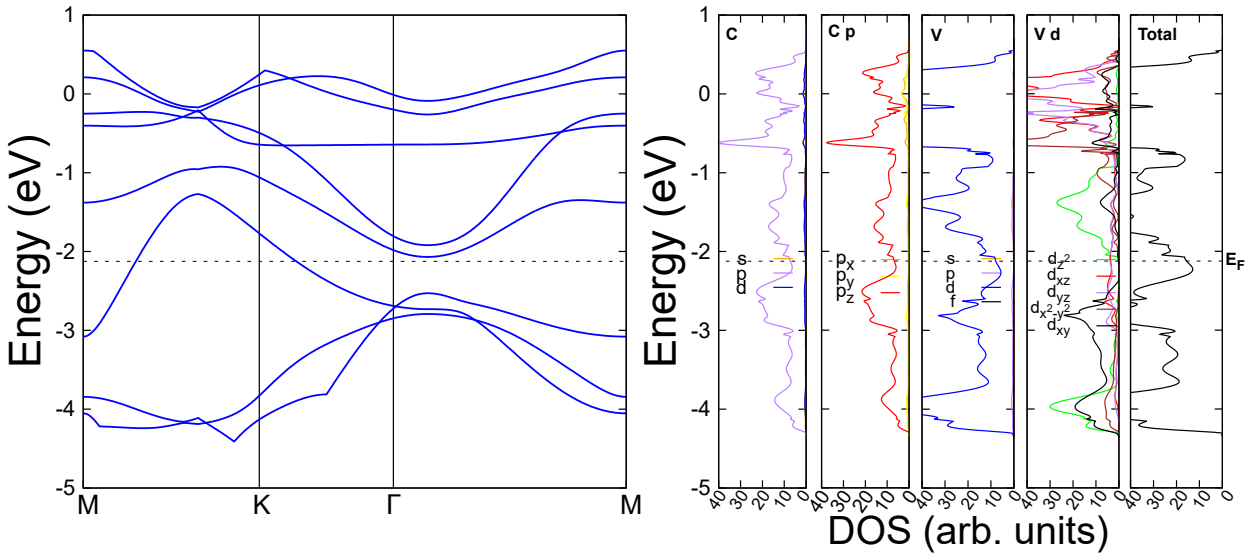


Figure S3: The band structure and DOSs of the alpha electron of AFM BLG-3V are presented. The individual components of the DOSs contributions from the C and V atoms, and total DOSs are also presented in here.

For the case of BLG-3V, there also exists one AFM conformation given the symmetry of the unit cell consisting of two Vanadium atoms with electrons in the alpha state and one in the beta state, or vice versa. We found that the AFM BLG-3V structure chooses to allocate the spin as -1.726 for the beta state Vanadium, and the two alpha state Vanadiums with spins of 1.098. The average spin of AFM BLG-3V is 0.405. The AFM structure of BLG-3V is slightly less favorable than to the FM structure by $\Delta G_f = 0.193$ eV. As for the electronic properties, we found for alpha and beta electrons that they are both highly conductive with a large DOSs and band overlap around the Fermi Energy (see Figure S3 and Figure S4) resulting in a large electron density around the E_F . The present calculations showed that both the FM and AFM states of BLG-3V material are conducting and thus they show ordinary metallic behavior. This study of spin behavior shows

that not only the electronic properties of BLG-intercalated materials dependent on the concentration of Vanadium atoms intercalated in BLG, but also on the arrangement of the spin, which adds an additional variable to modifying the behavior of BLG-intercalated materials.

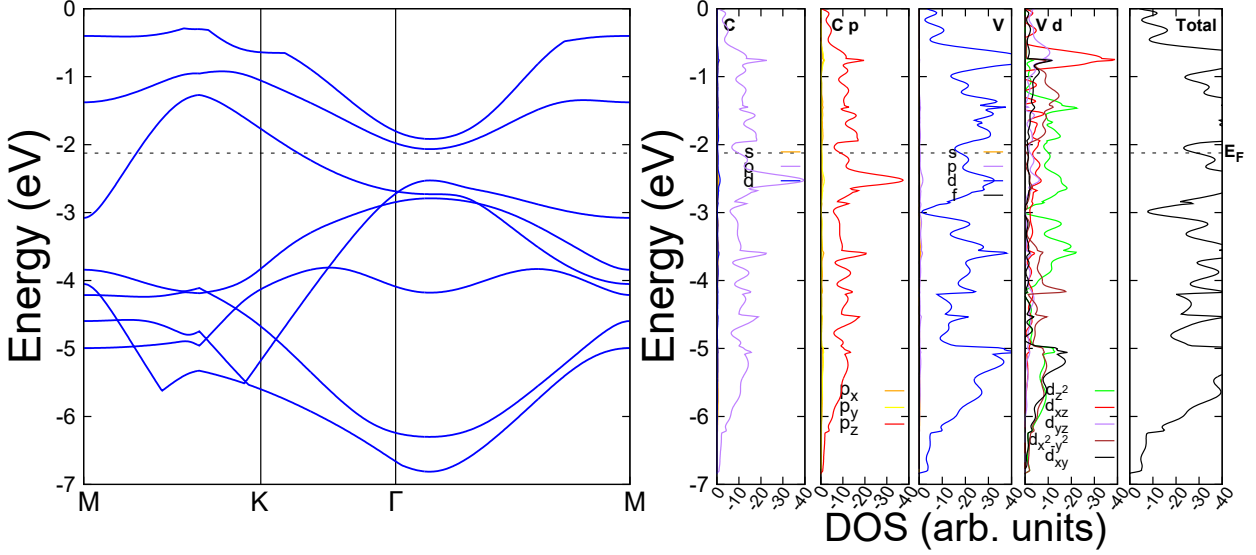


Figure S4: The band structure and DOSs of the beta electron of AFM BLG-3V are presented. The individual components of the DOSs contributions from the C and V atoms, and total DOSs are also presented here. Just as the alpha electrons, we can see the conductive behavior for the beta electrons.

Thus, we show an alternative method of controlling the electronic properties of BLG-intercalated material is by altering the spin conformation. The AFM arrangement of spins in the BLG-2V material changes it from a metal to a semi-conductor with a small band gap. And for the BLG-3V material, the AFM state changes the electron density around the Fermi level compared FM states. We have observed that the $3d$ orbitals of V receive more electron donation from the graphene $2p_z$ sub-shell when the total spin is increased. We have found the $2p_z$ sub-shell of p -orbital of C atoms and $3d_{yz}$ sub-shell of d -orbital of V atoms account for the largest electron contribution in total DOSs.

Table S2: Bond distances and lattice constants of the BLG-1Nb, and BLG-1Ta 2D materials. The d is defined as the intercalation distance between the layers.

Component	C-C (Å)	C-Nb/C-Ta (Å)	a (Å)	b (Å)	d (Å)
BLG-1V	1.439	2.243	4.942	4.942	3.441
BLG-1Nb	1.439	2.313	4.950	4.950	3.600
BLG-1Ta	1.445	2.284	4.952	4.952	3.522

4 Optimized Structures (.cif format)

The optimized structures are provided below in .cif format.

4.1 MLG: Monolayer Graphene

data_MLG


```

_symmetry_space_group_name_H-M      'P6/MMM'
_symmetry_Int_Tables_number         191
_symmetry_cell_setting               hexagonal
loop_
_symmetry_equiv_pos_as_xyz
  x,y,z
  -y,x-y,z
  -x+y,-x,z
  -x,-y,z
  y,-x+y,z
  x-y,x,z
  y,x,-z
  x-y,-y,-z
  -x,-x+y,-z
  -y,-x,-z
  -x+y,y,-z
  x,x-y,-z
  -x,-y,-z
  y,-x+y,-z
  x-y,x,-z
  x,y,-z
  -y,x-y,-z
  -x+y,-x,-z
  -y,-x,z
  -x+y,y,z
  x,x-y,z
  y,x,z
  x-y,-y,z
  -x,-x+y,z
_cell_length_a                       2.4515
_cell_length_b                       2.4515
_cell_length_c                       500.0000
_cell_angle_alpha                    90.0000
_cell_angle_beta                     90.0000
_cell_angle_gamma                    120.0000
loop_
_atom_site_label
_atom_site_type_symbol
_atom_site_fract_x
_atom_site_fract_y
_atom_site_fract_z
_atom_site_U_iso_or_equiv
_atom_site_adp_type
_atom_site_occupancy
C001  C      0.33333  -0.33333  0.00000  0.00000  Uiso  1.00

```

4.2 AA-BLG: AA-stacked Bilayer Graphene

```

data_AA-Stacked-BLG
_symmetry_space_group_name_H-M      'P6/MMM'
_symmetry_Int_Tables_number         191
_symmetry_cell_setting               hexagonal
loop_
_symmetry_equiv_pos_as_xyz
  x,y,z

```

```

-y,x-y,z
-x+y,-x,z
-x,-y,z
y,-x+y,z
x-y,x,z
y,x,-z
x-y,-y,-z
-x,-x+y,-z
-y,-x,-z
-x+y,y,-z
x,x-y,-z
-x,-y,-z
y,-x+y,-z
x-y,x,-z
x,y,-z
-y,x-y,-z
-x+y,-x,-z
-y,-x,z
-x+y,y,z
x,x-y,z
y,x,z
x-y,-y,z
-x,-x+y,z
_cell_length_a          2.4490
_cell_length_b          2.4490
_cell_length_c          500.0000
_cell_angle_alpha       90.0000
_cell_angle_beta        90.0000
_cell_angle_gamma       120.0000
loop_
_atom_site_label
_atom_site_type_symbol
_atom_site_fract_x
_atom_site_fract_y
_atom_site_fract_z
_atom_site_U_iso_or_equiv
_atom_site_adp_type
_atom_site_occupancy
C001  C    -0.66667  -0.33333  0.00320  0.00000  Uiso  1.00

```

4.3 AB-BLG: AB-stacked Bilayer Graphene

```

data_AB-Stacked-BLG
_symmetry_space_group_name_H-M  'P-3M1'
_symmetry_Int_Tables_number     164
_symmetry_cell_setting          trigonal
loop_
_symmetry_equiv_pos_as_xyz
  x,y,z
  -y,x-y,z
  -x+y,-x,z
  y,x,-z
  x-y,-y,-z
  -x,-x+y,-z
  -x,-y,-z

```

```

y,-x+y,-z
x-y,x,-z
-y,-x,z
-x+y,y,z
x,x-y,z
_cell_length_a          2.4491
_cell_length_b          2.4491
_cell_length_c          500.0000
_cell_angle_alpha       90.0000
_cell_angle_beta        90.0000
_cell_angle_gamma       120.0000
loop_
_atom_site_label
_atom_site_type_symbol
_atom_site_fract_x
_atom_site_fract_y
_atom_site_fract_z
_atom_site_U_iso_or_equiv
_atom_site_adp_type
_atom_site_occupancy
C001  C    0.00000  0.00000  0.00304  0.00000  Uiso  1.00
C003  C   -0.33333  0.33333  0.00304  0.00000  Uiso  1.00

```

4.4 BLG-1V: BLG-intercalated with 1 V

```

data_BLG-1V
_symmetry_space_group_name_H-M  'P6/MMM'
_symmetry_Int_Tables_number     191
_symmetry_cell_setting          hexagonal
loop_
_symmetry_equiv_pos_as_xyz
x,y,z
-y,x-y,z
-x+y,-x,z
-x,-y,z
y,-x+y,z
x-y,x,z
y,x,-z
x-y,-y,-z
-x,-x+y,-z
-y,-x,-z
-x+y,y,-z
x,x-y,-z
-x,-y,-z
y,-x+y,-z
x-y,x,-z
x,y,-z
-y,x-y,-z
-x+y,-x,-z
-y,-x,z
-x+y,y,z
x,x-y,z
y,x,z
x-y,-y,z
-x,-x+y,z

```

```

_cell_length_a          4.9423
_cell_length_b          4.9423
_cell_length_c          500.0000
_cell_angle_alpha       90.0000
_cell_angle_beta        90.0000
_cell_angle_gamma       120.0000
loop_
_atom_site_label
_atom_site_type_symbol
_atom_site_fract_x
_atom_site_fract_y
_atom_site_fract_z
_atom_site_U_iso_or_equiv
_atom_site_adp_type
_atom_site_occupancy
C001  C    -0.33601  -0.16801  0.00344  0.00000  Uiso  1.00
C007  C     0.33333  -0.33333  0.00339  0.00000  Uiso  1.00
V009  V     0.00000   0.00000  0.00000  0.00000  Uiso  1.00

```

4.5 BLG-2V: BLG-intercalated with 2 V

```

data_BLG-2V
_symmetry_space_group_name_H-M  'CMM2'
_symmetry_Int_Tables_number     35
_symmetry_cell_setting          orthorhombic
loop_
_symmetry_equiv_pos_as_xyz
  x,y,z
  -x,-y,z
  x,-y,z
  -x,y,z
  x+1/2,y+1/2,z
  -x+1/2,-y+1/2,z
  x+1/2,-y+1/2,z
  -x+1/2,y+1/2,z
_cell_length_a          5.0217
_cell_length_b          8.5748
_cell_length_c          500.0000
_cell_angle_alpha       90.0000
_cell_angle_beta        90.0000
_cell_angle_gamma       90.0000
loop_
_atom_site_label
_atom_site_type_symbol
_atom_site_fract_x
_atom_site_fract_y
_atom_site_fract_z
_atom_site_U_iso_or_equiv
_atom_site_adp_type
_atom_site_occupancy
C001  C     0.24997   0.08385  -0.00854  0.00000  Uiso  1.00
C010  C     0.24996   0.08385  -0.00125  0.00000  Uiso  1.00
C005  C     0.00000  -0.16606  -0.00840  0.00000  Uiso  1.00
C007  C     0.00000  -0.33405  -0.00840  0.00000  Uiso  1.00
C014  C     0.00000  -0.16608  -0.00139  0.00000  Uiso  1.00

```

C016	C	0.00000	-0.33403	-0.00139	0.00000	Uiso	1.00
V009	V	0.00000	0.00000	-0.00490	0.00000	Uiso	1.00
V018	V	0.50000	0.00000	-0.00490	0.00000	Uiso	1.00

4.6 BLG-3V: BLG-intercalated with 3 V

```

data_BLG-3V
_symmetry_space_group_name_H-M      'P6/MMM'
_symmetry_Int_Tables_number         191
_symmetry_cell_setting               hexagonal
loop_
_symmetry_equiv_pos_as_xyz
  x,y,z
  -y,x-y,z
  -x+y,-x,z
  -x,-y,z
  y,-x+y,z
  x-y,x,z
  y,x,-z
  x-y,-y,-z
  -x,-x+y,-z
  -y,-x,-z
  -x+y,y,-z
  x,x-y,-z
  -x,-y,-z
  y,-x+y,-z
  x-y,x,-z
  x,y,-z
  -y,x-y,-z
  -x+y,-x,-z
  -y,-x,z
  -x+y,y,z
  x,x-y,z
  y,x,z
  x-y,-y,z
  -x,-x+y,z
_cell_length_a                       5.0319
_cell_length_b                       5.0319
_cell_length_c                       20.0000
_cell_angle_alpha                    90.0000
_cell_angle_beta                     90.0000
_cell_angle_gamma                    120.0000
loop_
_atom_site_label
_atom_site_type_symbol
_atom_site_fract_x
_atom_site_fract_y
_atom_site_fract_z
_atom_site_U_iso_or_equiv
_atom_site_adp_type
_atom_site_occupancy
C001  C      0.33575  0.16787  0.08988  0.00000  Uiso  1.00
C013  C     -0.33333  0.33333  0.09613  0.00000  Uiso  1.00
V017  V      0.50000  0.00000  0.00000  0.00000  Uiso  1.00

```

4.7 BLG-1Nb: BLG-intercalated with 1 Nb

```

data_BLG-1Nb
_symmetry_space_group_name_H-M      'P6/MMM'
_symmetry_Int_Tables_number         191
_symmetry_cell_setting              hexagonal
loop_
_symmetry_equiv_pos_as_xyz
  x,y,z
  -y,x-y,z
  -x+y,-x,z
  -x,-y,z
  y,-x+y,z
  x-y,x,z
  y,x,-z
  x-y,-y,-z
  -x,-x+y,-z
  -y,-x,-z
  -x+y,y,-z
  x,x-y,-z
  -x,-y,-z
  y,-x+y,-z
  x-y,x,-z
  x,y,-z
  -y,x-y,-z
  -x+y,-x,-z
  -y,-x,z
  -x+y,y,z
  x,x-y,z
  y,x,z
  x-y,-y,z
  -x,-x+y,z
_cell_length_a                      4.9443
_cell_length_b                      4.9443
_cell_length_c                      500.0000
_cell_angle_alpha                   90.0000
_cell_angle_beta                    90.0000
_cell_angle_gamma                   120.0000
loop_
_atom_site_label
_atom_site_type_symbol
_atom_site_fract_x
_atom_site_fract_y
_atom_site_fract_z
_atom_site_U_iso_or_equiv
_atom_site_adp_type
_atom_site_occupancy
C001  C    -0.33600  -0.16800  0.09050  0.00000  Uiso  1.00
C013  C     0.33333  -0.33333  0.08851  0.00000  Uiso  1.00
NB017 Nb    0.00000   0.00000  0.00000  0.00000  Uiso  1.00

```

4.8 BLG-1Ta: BLG-intercalated with 1 Ta

```

data_BLG-1Ta
_symmetry_space_group_name_H-M      'P6/MMM'
_symmetry_Int_Tables_number         191

```

```

_symmetry_cell_setting      hexagonal
loop_
_symmetry_equiv_pos_as_xyz
  x,y,z
  -y,x-y,z
  -x+y,-x,z
  -x,-y,z
  y,-x+y,z
  x-y,x,z
  y,x,-z
  x-y,-y,-z
  -x,-x+y,-z
  -y,-x,-z
  -x+y,y,-z
  x,x-y,-z
  -x,-y,-z
  y,-x+y,-z
  x-y,x,-z
  x,y,-z
  -y,x-y,-z
  -x+y,-x,-z
  -y,-x,z
  -x+y,y,z
  x,x-y,z
  y,x,z
  x-y,-y,z
  -x,-x+y,z
_cell_length_a             4.9465
_cell_length_b             4.9465
_cell_length_c             500.0000
_cell_angle_alpha          90.0000
_cell_angle_beta           90.0000
_cell_angle_gamma          120.0000
loop_
_atom_site_label
_atom_site_type_symbol
_atom_site_fract_x
_atom_site_fract_y
_atom_site_fract_z
_atom_site_U_iso_or_equiv
_atom_site_adp_type
_atom_site_occupancy
C001  C    -0.33620 -0.16810  0.08858  0.00000  Uiso  1.00
C013  C     0.33333 -0.33333  0.08610  0.00000  Uiso  1.00
TA017 Ta   0.00000  0.00000  0.00000  0.00000  Uiso  1.00

```